

Three-Dimensional Warping Registration of the Pelvis and Prostate

Baowei Fei ^{a*}, Corey Kemper ^a, David L Wilson ^{ab**}

^a Department of Biomedical Engineering, Case Western Reserve University, OH 44106

^b Department of Radiology, University Hospitals of Cleveland, OH 44106

ABSTRACT

We are investigating interventional MRI guided radiofrequency (RF) thermal ablation for the minimally invasive treatment of prostate cancer. Among many potential applications of registration, we wish to compare registered MR images acquired before and immediately after RF ablation in order to determine whether a tumor is adequately treated. Warping registration is desired to correct for potential deformations of the pelvic region and movement of the prostate. We created a two-step, three-dimensional (3D) registration algorithm using mutual information and thin plate spline (TPS) warping for MR images. First, automatic rigid body registration was used to capture the global transformation. Second, local warping registration was applied. Interactively placed control points were automatically optimized by maximizing the mutual information of corresponding voxels in small volumes of interest and by using a 3D TPS to express the deformation throughout the image volume. Images were acquired from healthy volunteers in different conditions simulating potential applications. A variety of evaluation methods showed that warping consistently improved registration for volume pairs whenever patient position or condition was purposely changed between acquisitions. A TPS transformation based on 180 control points generated excellent warping throughout the pelvis following rigid body registration. The prostate centroid displacement for a typical volume pair was reduced from 3.4 mm to 0.6 mm when warping was added.

Keywords: Warping image registration, medical imaging, interventional magnetic resonance imaging (iMRI), mutual information, thin plate spline, prostate cancer.

1. INTRODUCTION

We are investigating three-dimensional (3D) image registration to be used in applications of prostate cancer diagnosis, staging, and therapy. In particular, we are interested in applications related to the minimally invasive interventional magnetic resonance imaging (iMRI) guided treatment of prostate cancer. At our institution, we currently use iMRI on a low-field open magnet system to guide radiofrequency (RF) thermal ablation of abdominal cancer,^{1,2} and we are investigating this method for prostate cancer treatment. A unique feature of iMRI-guided thermal ablation is that therapy can be monitored with MR either by acquiring images of the thermally induced lesion or by measuring temperature. In addition, MR imaging of the prostate is desirable because it more accurately delineates the prostate than does CT,^{3,4} which can overestimate the prostate volume,^{5,6} and ultrasound, which has a tendency to underestimate the extent of lesions.⁷

Several applications in prostate imaging require registration. First, comparison of registered MR images acquired before and immediately after RF ablation can be used to determine whether a tumor is adequately treated. This is

* BXF18@po.cwru.edu, ** DLW@po.cwru.edu, Wickenden Building 319, 10900 Euclid Avenue, Cleveland, OH 44106.

particularly helpful in instances where the edematous response to treatment can be confused with a highly perfused tumor. Second, registration of serial examinations can be used to follow regression/progression of tumor. Third, incorporating the functional, biochemical images into the iMRI paradigm will aid image-guided treatments, as recently reported by us.^{8,9}

Several reports describe methods for registration in the pelvis or prostate.¹⁰⁻¹⁵ These methods required either segmentation or visual identification of structures and they were based on rigid body transformation. We recently reported a mutual information rigid body transformation method for prostate registration.¹⁶ For volume pairs acquired over a short time span from a supine subject with legs flat on the table, registration accuracy of both prostate centroids (typically < 1 mm) and bony landmarks (average 1.6 mm) was on the order of a voxel (≈ 1.4 mm). We obtained somewhat larger prostate registration errors of about 3.0 mm when volume pairs were obtained under very different conditions, e.g., legs flat and legs raised, or with and without bladder or rectal filling. Rigid body registration of the pelvis cannot follow prostate movements due to changes in the postures of legs and deformation of the bladder and rectum, as reported by us¹⁶ and others.^{14,17}

There are a number of reports on warping registration.¹⁸⁻²⁰ These applications were mainly on the brain and breast; and far few described results for the abdomen.^{21,22} For our application, we are developing voxel-based warping registration in the pelvis and prostate.

There are challenges to the pelvis and prostate registration. First, pelvic regions can change shape significantly, unlike the brain to which registration has been most often applied. Different patient positions such as displacement of the legs can cause the movement and deformation of internal organs. Second, the normal prostate is a small organ that when healthy measures only about 3.8 cm in its widest dimension transversely across the base.²³ Third, the prostate might move relative to the pelvic bones due to changes in bladder and rectal filling.^{14,17}

In the present study, we perform experiments to determine if warping can improve registration of pelvic MR. High quality, 3D MR image volumes from a commercially available 1.5 T system are used to determine the best possible results. We examine conditions found in the potential clinical applications described previously. We will qualitatively and quantitatively compare results of warping and rigid body registration using 9 volume pairs from three volunteers.

2. REGISTRATION ALGORITHM

2.1. Similarity Measurements

We used two similarity measures, mutual information and correlation coefficient (CC), in our registration. One volume R is the *reference*, and the other F is *floating*. Their mutual information $MI(R, F)$ is given below.²⁴

$$MI(R, F) = \sum_{r, f} p_{RF}(r, f) \log \frac{p_{RF}(r, f)}{p_R(r) \cdot p_F(f)}$$

The joint probability $p_{RF}(r, f)$ and the marginal probabilities $p_R(r)$ of the reference image and $p_F(f)$ of the floating image, can be estimated from the normalized joint intensity histograms. When two images are geometrically aligned, MI is maximal.²⁴ The correlation coefficient $CC(R, F)$ is given below.²⁵

$$CC(R, F) = \frac{\sum (R(r) - \bar{R}(r))(F(f) - \bar{F}(f))}{\sqrt{\sum (R(r) - \bar{R}(r))^2 \sum (F(f) - \bar{F}(f))^2}}$$

Here $\overline{R}(r)$, $\overline{F}(f)$ denote the average intensities of the reference and floating volumes and the summation includes all voxels within the overlap of both volumes.

2.2. Rigid Body Registration Algorithm with Special Features

The rigid body registration algorithm includes special features to improve robustness for MR pelvic images. Reference is matched to the *reformatted* volume obtained by transforming the floating volume. We use a multi-resolution approach and perform registration from low to high resolution. At low resolution, we resample both images at 1/4 or 1/2 number of voxels along each linear dimension, respectively. A simplex algorithm varies the six rigid body transformation parameters (three translations and three angles) to optimize the similarity measure.²⁶ We use CC at the two lower resolutions because it gives fewer local maximums^{8,9,16} and because it can be calculated faster than MI. We use MI at full resolution because the peaked similarity function gives a more precise solution than CC.^{9,16} To avoid local maximums, we include a restarting feature where registration is restarted with randomly perturbed parameters. The algorithm restarts until the absolute CC is above an experimentally determined threshold or the maximum number of restarts is reached. Absolute CC is used for the restart test rather than MI because CC has fewer problems with local and incorrect global maximums at low resolution.^{9,16}

We record all important results following an optimization cycle including the CC and/or MI values, the number of restarts, and the transformation parameters. At the end of processing at a lower resolution, we always select the transformation parameters having the maximum CC value. We then scale the translation parameters appropriately and assign the new parameters to be initial values at the next higher resolution. At the highest resolution, we select the final transformation parameters to be those with the maximum MI value.

Typical parameter values are now described. We use an initial guess at the lowest resolution of all zeros because the patient is normally oriented approximately the same way from one scan to the next. Based on experience, we set the CC thresholds at 0.50, 0.55, and 0.65, and the maximum numbers of restarts at 10, 5, and 3, from low to high resolution, respectively.

2.3. Warping Registration Using Optimized Control Points

The warping registration algorithm includes three major steps: control point (CP) selection, control point optimization, and thin plate spline (TPS) warping. Again, the unchanging volume is the *reference*, and the one to be warped is *floating*.

The manual selection of CP's is an important step. We used *RegViz*, a program written in IDL (Interactive Data Language, Research System Inc., Boulder, CO) and created in our laboratory for visualizing and analyzing image volumes. Following rigid body registration, the aligned two volumes are displayed in two rows slice-by-slice. Corresponding CP's in the two volumes are placed using a cursor, and sometimes they are in different image slices. The 3D coordinates are automatically stored in a file. Because of the optimization that occurs later, the correspondence can be up to 15 mm or ≈ 10 voxels in error. More experience with CP selection is described in Results. Typically, we used 180 CP's for a volume with 256 x 256 x 140 isotropic voxels.

The next step of the warping algorithm is the CP optimization. We define a small cubic volume of interest (VOI) centered at each CP. The VOI can be 16 or 64 voxels on a side. A simplex optimization algorithm varies the x, y, and z transformation parameters of the floating VOI until the mutual information with the reference VOI is optimized. Each control point is optimized independently.

The final major step is to warp the floating volume using the optimal CP's coordinates to establish a TPS transformation. We extended the two-dimensional TPS transformation method reported by Bookstein²⁷ to three dimensions in a manner similar to that of Davis et al.¹⁹

2.4. Additional Details

There are several preprocessing details. The input MRI volume is a 3D MR acquisition giving 256 x 256 x 128 nearly isotropic voxels over a field of view covering the whole pelvis. We create isotropic voxels of about 1.4 mm on a side using 3D linear interpolation. From the top and bottom of the volume, we optionally crop transverse slices that are over 35 mm away from the prostate rim. Cropping is done to remove slices having reduced brightness due to sensitivity fall off from the receiver coils and/or artifacts from a small field of view. For both rigid body registration and VOI optimization, we use trilinear interpolation. Optimization of similarity ends either when the maximum number of calculations is reached (typically 500) or the fractional change in the similarity function is smaller than a tolerance (typically 0.001). We use IDL as the programming language.

3. EXPERIMENTAL METHODS

3.1. Image Acquisition

All MRI volumes were acquired using a 1.5 T Siemens MRI system (Magnetom Symphony, Siemens Medical Systems, Erlangen, Germany). An 8-element phased array body coil was used to ensure coverage of the prostate with a uniform sensitivity. Typically two anterior and two posterior elements were enabled for signal acquisition. We used two different MR sequences. First, we used a 3D RF spoiled gradient echo steady state pulse sequence (FLASH) with TR/TE/flip parameters of 12/5.0/60 which give 256 x 256 x 128 voxels over a 330 x 330 x 256-mm field of view (FOV) to yield 1.3 x 1.3 x 2.0-mm voxels oriented to give the highest resolution for transverse slices. The acquisition time was 5.6 min. This sequence was good for pelvic imaging but was not ideal for the prostate. Second, we used a 3D rapid gradient echo sequence (PSIF) designed to acquire the spin-echo component of the steady state response, rather than the free induction decay. The spin echo component formed immediately prior to the RF pulse, and it was shifted toward the prior RF pulse through appropriate gradient waveform design. The sequence with 9.4/5.0/60 (TR/TE/flip) yielded 160 x 256 x 128 voxels over a 219 x 350 x 192-mm rectangular FOV and 1.4 x 1.4 x 1.5-mm voxels oriented to give the highest resolution for transverse slices. There was over sampling at 31% in the slice direction to reduce aliasing artifacts. The acquisition time was 4.3 min. Most often, we used the second sequence, which gave excellent image contrast for the prostate and its surroundings.

3.2. Imaging Experiments

We acquired 3D MRI volume images from three normal volunteers under a variety of conditions simulating anticipated conditions in diagnostic and treatment applications. Before image acquisition, each volunteer drank water and had a relatively *full bladder*. In the *diagnostic position*, the subject laid supine throughout MR scanning. In the *treatment position*, the subject was supine, and his legs were supported at 30°-60° relative to the horizon and separated in a “V” with an angle of 60°-90° between two legs. This position should provide access for needle insertion in brachytherapy or RF thermal ablation. In some experiments, the subject micturated to create an *empty bladder* prior to imaging. For each subject, image volumes were obtained on the same day within one imaging session. Between volume acquisitions,

volunteers got off the MRI table, stretched, and walked around to ensure that they would assume a different position when they laid back on the table. All images of a volunteer were acquired with the same MRI acquisition parameters so as to ensure very similar gray values. In total, there are 3 volumes for each volunteer.

3.3. Volume Pairs for Registration

We registered 9 volume pairs under different conditions. Three pairs are *treatment-diagnosis*; three pairs are *full-empty bladder*; and three pairs are *diagnosis-diagnosis*. Rigid body and warping registration were applied to each of the volume pairs. Results were evaluated as described next.

3.4. Registration Evaluation

We used the multiple visualization features of RegViz to visually evaluate registration results. First, we manually segmented prostate boundaries in image slices and copied them to corresponding slices from the other volume. This enabled visual determination of the overlap of prostate boundaries over the entire volume. We applied the same method to evaluate pelvic registration. Second, color overlay displays were used to evaluate overlap of structures. One image was rendered in gray and the other in the “hot - iron” color scheme available in IDL. To visualize potential differences, it was quite useful to interactively change the contribution of each image using the transparency scale. Third, we used a sector display, which divided the reference and registered images into rectangular sectors and created an output image by alternating sectors from the two input images. Even subtle shifts of edges could be clearly seen.¹⁶

Voxel gray value measures were calculated as indicators of registration quality. Mutual information and correlation coefficient between registered volumes were computed. The higher the MI values, the more likely the two volumes are well registered. Since volumes to be registered were acquired using the same acquisition parameters, high absolute CC values were obtained when registration was good.²⁰ Because voxel intensities were comparable, we created difference images and calculated statistics such as the voxel mean and standard deviation following registration.

Finally, to assess prostate registration error, we measured potential displacements of the 3D centroid of the prostate. We used RegViz to manually segment the prostate across all image slices and calculated the 3D centroid. A similar method was used by West et al. to evaluate rigid body registration of the brain.²⁸

4. RESULTS AND DISCUSSION

4.1. Control Point Selection

In well over 50 registration experiments, we investigated the number and placement of CP's on warping registration quality. We quickly determined that many CP's are required in order to get good visual matching of our very high-resolution MR images showing great anatomical detail, especially when large deformations occurred as in the case of diagnosis-treatment. We progressively increased the number of CP's from 15 to 250. We found that less than 120 CP's did not produce smooth and reasonable warps. Warping with 180 CP's excellently approximated the deformation of the pelvis and internal organs. More than 220 CP's did not give significant improvement but needed more time for manual selection and optimization. As a result of this experience, we modified the registration method to be more suitable for many CP's (see Section 2).

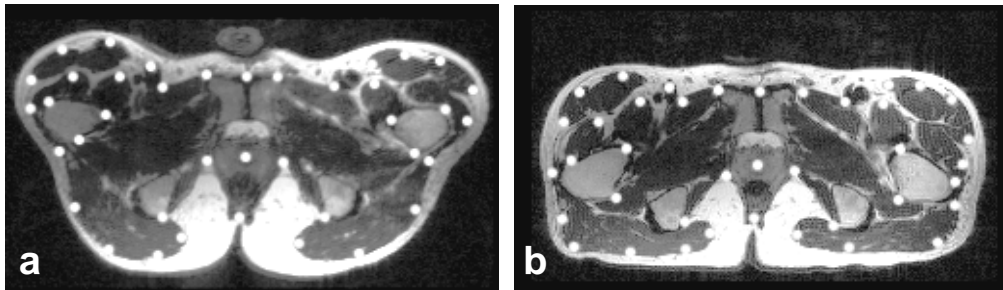


Figure 1. Control point selection when images are acquired in the treatment and diagnostic positions. Image (a) is from the reference volume acquired in the treatment position with legs raised. Image (b) is to be warped and is from the volume acquired in the diagnostic position with the subject supine on the table. Transverse slices best show the deformations, especially at the legs. As described in the text, control points indicated by the white dots are selected around the pelvic surface and the prostate. Each control point is located at one voxel but displayed much bigger for better visualization. Volumes are from volunteer S2.

We also determined that it was necessary to place the CP's in strategic locations, and some rules follow. For registration of treatment and diagnostic image volumes, most CP's were selected using transverse slices because they best showed the pelvic displacement when moving the legs to the treatment position (Figure 1). About 30 CP pairs were placed near edge and point features having recognizable correspondence on each of 5-8 transverse slices with a z interval of ~ 8 mm, covering the entire prostate region. Additionally, we placed about 25 CP's from sagittal slices because they provided other structures that can be missed in the transverse images. It was also important to include CP's from organs other than the prostate because they constrained warps. We always placed CP's at critical regions such as the prostate center, pelvic surface, bladder border, and rectal walls.

4.2. Registration Quality of Warping and Rigid Body Registration

In Figure 2, we compare warping and rigid body registration for a typical volume pair in the treatment and diagnostic positions. Using rigid body registration, there is significant misalignment throughout large regions in the pelvis (Figure 2a) that is greatly reduced with warping (Figure 2b). Note that warping even allows the outer surfaces to match well. Other visualization methods such as two-color overlays and difference images, quickly show matching of structures without segmentation but do not reproduce well on a printed page. The prostate 3D centroid calculated from segmented images displaced by only 0.6 mm, or 0.4 voxels, following warping. Following rigid body registration, the prostate was misaligned with a displacement to the posterior of ≈ 3.4 mm when in the treatment position

We examined the effect of conditions such as bladder and rectal filling that might change from one imaging session to the next (not shown). Contour overlap showed that warping registration perfectly aligns the prostate while rigid body does not. In addition, rigid body registration does not align the bladder. With warping, the bladder perfectly matches the reference. Other visualization methods showed excellent alignment of internal and surface edges. Difference images show that warping greatly improves alignment of internal structures as compared to rigid body registration.

We also examined volume pairs with both volumes acquired in the diagnostic position under comparable conditions. In all such cases, rigid body registration worked as well as warping. There were no noticeable deformations in the pelvis, and prostate centroids typically displaced less than 1.0 mm between the two registered volumes.

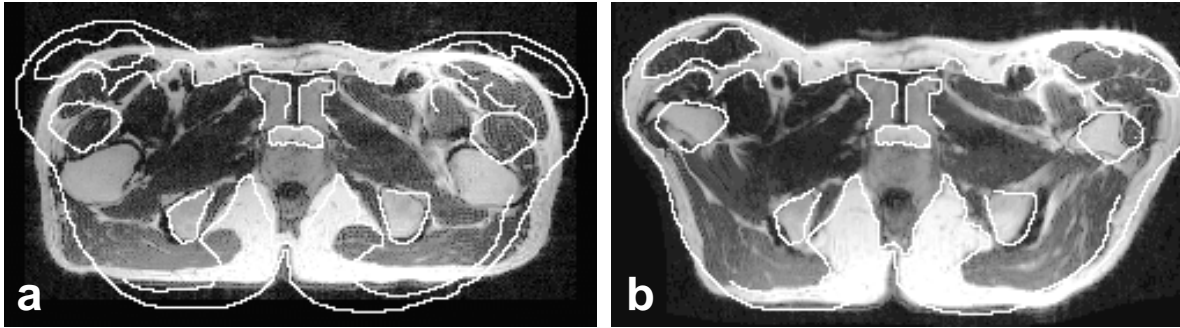


Figure 2. Comparison of warping and rigid body registration for volumes acquired in the treatment and diagnostic positions. Image (a) is from the floating volume acquired in the diagnostic position following rigid body registration. Pelvic contours manually segmented from the reference show significant misalignment. Image (b) is from the floating volume acquired in the diagnostic position following warping registration. The misalignment is greatly improved with warping. Images are transverse slices from subject S2.

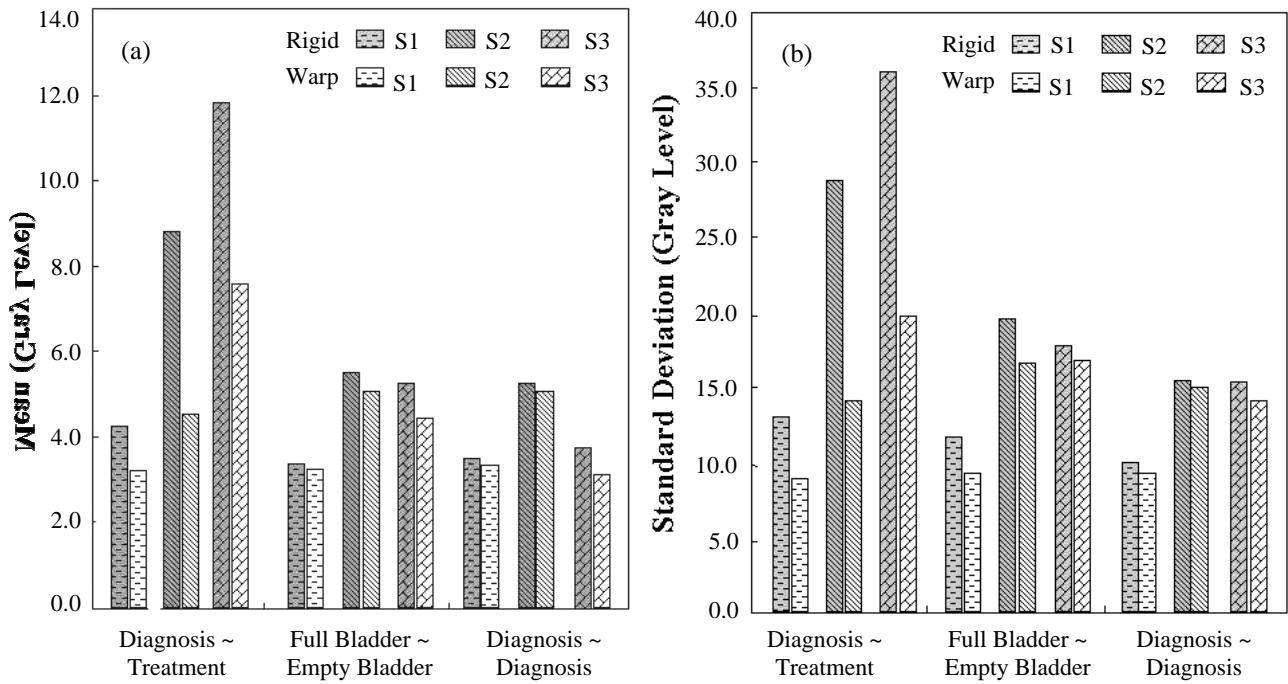


Figure 3. Image statistics of absolute intensity difference images for rigid body and warping registration. The mean (a) and standard deviation (b) are plotted. See the legend of Figure 3 for other details. Warping decreased the mean and standard deviation in each case, but the most significant decreases occurred in the case of the treatment-diagnosis volume pairs.

4.3. Quantitative Evaluation of Warping Registration

Statistics of image differences following rigid body and warping registration are shown in Figure 3. Warping reduces the absolute intensity difference between corresponding voxels (Figure 3a). We did not use non-absolute differences as evaluation criteria because the positive and negative differences can be canceled. The standard deviation of absolute difference is also reduced (Figure 3b). We also calculated the correlation coefficient and mutual information values between registered volumes. Warping increased CC and MI values in every case.

4.4. Algorithmic Robustness and Efficiency

The rigid body algorithm gives robust registration. Because of two principal design features, the algorithm is quite robust and accurate for volume pairs acquired in the same positions and with comparable conditions.¹⁶ First, using both CC and MI at different resolutions was an important feature that increased robustness. CC gave fewer local minimums at low resolutions and MI was more accurate at high resolution.^{8,9} Second, the restarting mechanism was also quite important. Without restarting, we found that registrations sometimes failed in cases of volumes with large mismatches and significant deformation. Even these cases resulted in a proper solution when restarting was employed. The time for rigid body registration, typically 5 minutes on a Pentium IV, 1.8 GHz CPU, with 1.0 GBytes of memory, could be greatly improved with C rather than IDL.

The interactive warping registration algorithm is designed to be very computationally efficient for TPS warping with hundreds of CP's. First, the optimization of small VOI's is very fast. Second, we optimized each CP separately because the optimization of three parameters (x , y , and z) is simple and fast. Third, we applied the TPS transformation once to the final, optimal CP's; this saved considerable time. Using the same computer above, for a volume with 256x256x140 voxels and 180 CP's, the warping registration typically takes about 15-45 minutes depending on the VOI size. If we were to use optimized C code, the total time for rigid body and warping registration should reduce to within 5 minutes.

5. CONCLUSION

The mutual information warping registration works better than rigid body registration whenever the subject position or condition is greatly changed between acquisitions. It will probably be a useful tool for many applications in prostate diagnosis, staging, and therapy. It is fast for hundreds of control points and can be applied to a variety of applications.

ACKNOWLEDGEMENTS

The algorithm developed in this research was supported by NIH grants R01-CA-84433-01 and R33-CA-88144-01.

REFERENCES

- 1 J.S.Lewin, C.F.Connell, J.L.Duerk, Y.C.Chung, M.E.Clampitt, J.Spisak, G.S.Gazelle, and J.R.Haaga, "Interactive MRI-guided radiofrequency interstitial thermal ablation of abdominal tumors: Clinical trial for evaluation of safety and feasibility," *Journal of Magnetic Resonance Imaging*, vol. 8, pp. 40-47, 1998.
- 2 E.M.Merkle, J.R.Shonk, J.L.Duerk, G.H.Jacobs, and J.S.Lewin, "MR-guided RF thermal ablation of the kidney in a porcine model," *American Journal of Roentgenology*, vol. 173, pp. 645-651, 1999.
- 3 K.Kagawa, W.R.Lee, T.E.Schultheiss, M.A.Hunt, A.H.Shaer, and G.E.Hanks, "Initial clinical assessment of CT-MRI image fusion software in localization of the prostate for 3D conformal radiation therapy," *International Journal of Radiation Oncology Biology Physics*, vol. 38, pp. 319-325, 1997.
- 4 M.Milosevic, S.Voruganti, R.Blend, H.Alasti, P.Warde, M.McLean, P.Catton, C.Catton, and M.Gospodarowicz, "Magnetic resonance imaging (MRI) for localization of the prostatic apex: comparison to computed tomography (CT) and urethrography," *Radiotherapy and Oncology*, vol. 47, pp. 277-284, 1998.
- 5 M.Roach, P.FaillaceAkazawa, C.Malfatti, J.Holland, and H.Hricak, "Prostate volumes defined by magnetic resonance imaging and computerized tomographic scans for three-dimensional conformal radiotherapy," *International Journal of Radiation Oncology Biology Physics*, vol. 35, pp. 1011-1018, 1996.
- 6 C.Rasch, I.Barillot, P.Remeijer, A.Touw, M.van Herk, and J.V.Lebesque, "Definition of the prostate in CT and MRI: A multi-observer study," *International Journal of Radiation Oncology Biology Physics*, vol. 43, pp. 57-66, 1999.
- 7 R.A.H.Boni, J.A.Boner, J.F.Debatin, F.Trinkler, H.Knonagel, A.Vonhochstetter, U.Helfenstein, and G.P.Krestin, "Optimization of prostate carcinoma staging - comparison of imaging and clinical methods," *Clinical Radiology*, vol. 50, pp. 593-600, 1995.
- 8 B.Fei, A.Wheaton, Z.Lee, K.Nagano, J.L.Duerk, and D.L.Wilson, "Robust registration algorithm for interventional MRI guidance for thermal ablation of prostate cancer," *Proceedings of SPIE Medical Imaging on Visualization, Display, and Image-Guided Procedures*, vol. 4319, pp. 53-60, 2001.
- 9 B.Fei, J.L.Duerk, and D.L.Wilson, "Slice to volume registration for interventional MRI guided treatment of prostate cancer," *IEEE Transactions on Medical Imaging*, (Submitted), 2001.
- 10 R.J.Hamilton, M.J.Blend, C.A.Pelizzari, B.D.Milliken, and S.Vijayakumar, "Using vascular structure for CT-SPECT registration in the pelvis," *Journal of Nuclear Medicine*, vol. 40, pp. 347-351, 1999.
- 11 J.M.Balter, H.M.Sandler, K.Lam, R.L.Bree, A.S.Lichter, and R.K.Ten Haken, "Measurement of prostate movement over the course of routine radiotherapy using implanted markers," *International Journal of Radiation Oncology Biology Physics*, vol. 31, pp. 113-118, 1995.
- 12 V.Narayana, P.L.Roberson, R.J.Winfield, and P.W.McLaughlin, "Impact of ultrasound and computed tomography prostate volume registration on evaluation of permanent prostate implants," *International Journal of Radiation Oncology Biology Physics*, vol. 39, pp. 341-346, 1997.
- 13 M.van Herk, J.C.de Munck, J.V.Lebesque, S.Muller, C.Rasch, and A.Touw, "Automatic registration of pelvic computed tomography data and magnetic resonance scans including a dull circle method for quantitative accuracy evaluation," *Medical Physics*, vol. 25, pp. 2054-2067, 1998.
- 14 M.vanHerk, A.Bruce, A.P.G.Kroes, T.Shouman, A.Touw, and J.V.Lebesque, "Quantification of organ motion during conformal radiotherapy of the prostate by three dimensional image registration," *International Journal of Radiation Oncology Biology Physics*, vol. 33, pp. 1311-1320, 1995.
- 15 A.M.Scott, H.A.Macapinlac, C.R.Divgi, J.J.Zhang, H.Kalaigian, K.Pentlow, S.Hilton, Graham.M.C, G.Sgouros, C.Pelizzari, G.Chen, J.Schlom, S.J.Goldsmith, and S.M.Larson, "Clinical validation of SPECT and CT/MRI image registration in radiolabeled monoclonal-antibody studies of colorectal carcinoma," *Journal of Nuclear Medicine*, vol. 35, pp. 1976-1984, 1994.
- 16 B.Fei, A.Wheaton, Z.Lee, J.L.Duerk, and D.L.Wilson, "Automatic MR volume registration and its evaluation for the pelvis and prostate," *Physics in Medicine and Biology*, (In Press), 2002.

- 17 R.K.Tenhaken, J.D.Forman, D.K.Heimbürger, A.Gerhardsson, D.L.Mcshan, C.Pereztamayo, S.L.Schoepfel, and A.S.Lichter, "Treatment planning issues related to prostate movement in response to differential filling of the rectum and bladder," *International Journal of Radiation Oncology Biology Physics*, vol. 20, pp. 1317-1324, 1991.
- 18 C.R.Meyer, J.L.Boes, B.Kim, P.H.Bland, K.R.Zasadny, P.V.Kison, K.Koral, K.A.Frey, and R.L.Wahl, "Demonstration of accuracy and clinical versatility of mutual information for automatic multimodality image fusion using affine and thin-plate spline warped geometric deformations," *Medical Image Analysis*, vol. 1, pp. 195-206, 1996.
- 19 M.H.Davis, A.Khotanzad, D.P.Flamig, and S.E.Harms, "A physics-based coordinate transformation for 3-D image matching," *IEEE Transactions on Medical Imaging*, vol. 16, pp. 317-328, 1997.
- 20 D.Rueckert, L.I.Sonoda, C.Hayes, D.L.G.Hill, M.O.Leach, and D.J.Hawkes, "Nonrigid registration using free-form deformations: Application to breast MR images," *IEEE Transactions on Medical Imaging*, vol. 18, pp. 712-721, 1999.
- 21 G.E.Christensen, P.Yin, M.W.Vannier, K.S.C.Chao, J.F.Dempsey, and J.F.Williamson, "Large-deformation image registration using fluid landmarks," Proceedings of 4th IEEE Southwest Symposium on Image Analysis and Interpretation, pp. 269-273, 2000.
- 22 D.L.Wilson, A.Carrillo, L.Zheng, A.Genc, J.L.Duerk, and J.S.Lewin, "Evaluation of 3D image registration as applied to MR-guided thermal treatment of liver cancer," *Journal of Magnetic Resonance Imaging*, vol. 8, pp. 77-84, 1998.
- 23 H.Gray, T.Pickering Pick, and R.Howden. *Gray Anatomy: The classic collector's edition*. New York: Gramercy Books, 1977.
- 24 F.Maes, A.Collignon, D.Vandermeulen, G.Marchal, and P.Suetens, "Multimodality image registration by maximization of mutual information," *IEEE Transactions on Medical Imaging*, vol. 16, pp. 187-198, 1997.
- 25 W.H.Press, B.P.Flannery, S.A.Teukolsky, and W.T.Vetterling. *Numerical Recipes in C: The Art of Scientific Computing, Second Edition*. New York: Cambridge University Press, 1993.
- 26 J.Nelder and R.A.Mead, "A simplex method for function minimization," *Computer Journal*, vol. 7, pp. 308-313, 1965.
- 27 F.L.Bookstein, "Principal warps - thin-plate splines and the decomposition of deformations," *IEEE Transactions on Pattern Analysis and Machine Intelligence*, vol. 11, pp. 567-585, 1989.
- 28 J.West, J.M.Fitzpatrick, M.Y.Wang, B.M.Dawant, C.R.Maurer, R.M.Kessler, R.J.Maciunas, C.Barillot, D.Lemoine, A.Collignon, F.Maes, P.Suetens, D.Vandermeulen, P.A.vandenElsen, S.Napel, T.S.Sumanaweera, B.Harkness, P.F.Hemler, D.L.G.Hill, D.J.Hawkes, C.Studholme, J.B.A.Maintz, M.A.Viergever, G.Malandain, X.Pennec, M.E.Noiz, G.Q.Maguire, M.Pollack, C.A.Pelizzari, R.A.Robb, D.Hanson, and R.P.Woods, "Comparison and evaluation of retrospective intermodality brain image registration techniques," *Journal of Computer Assisted Tomography*, vol. 21, pp. 554-566, 1997.

Baowei Fei, Corey Kemper, and David L. Wilson, "Three-dimensional warping registration of the pelvis and prostate", Milan Sonka, J. Michael Fitzpatrick, Editor, Proc. SPIE 4684, 528 (2002)

Copyright 2002 Society of Photo-Optical Instrumentation Engineers (SPIE). One print or electronic copy may be made for personal use only. Systematic reproduction and distribution, duplication of any material in this paper for a fee or for commercial purposes, or modification of the content of the paper are prohibited.

<http://dx.doi.org/10.1117/12.467195>